DESY 16-129

Overcoming the sign problem in 1-dimensional QCD by new integration rules with polynomial exactness

A. Ammon[d], T. Hartung[b], K. Jansen[a], H. Leövey[c], J. Volmer[a]

[a] *NIC, DESY Zeuthen, Platanenallee 6, D-15738 Zeuthen, Germany*
[b] *Department of Mathematics, King's College London, Strand, London WC2R 2LS, United Kingdom*
[c] *Institut für Mathematik, Humboldt-Universität zu Berlin, Unter den Linden 6, D-10099 Berlin*
[d] *IVU Traffic Technologies AG, Bundesallee 88, 12161 Berlin, Germany*

Abstract

In this paper we describe a new integration method for the groups $U(N)$ and $SU(N)$, for which we verified numerically that it is polynomially exact for $N \leq 3$. The method is applied to the example of 1-dimensional QCD with a chemical potential. We explore, in particular, regions of the parameter space in which the sign problem appears due the presence of the chemical potential. While Markov Chain Monte Carlo fails in this region, our new integration method still provides results for the chiral condensate on arbitrary precision, demonstrating clearly that it overcomes the sign problem. Furthermore, we demonstrate that our new method leads to orders of magnitude reduced errors also in other regions of parameter space.

Keywords: sign problem, polynomially exact integration, 1-dimensional QCD, chemical potential, lattice systems

1. Introduction

The sign problem in models of statistical and high energy physics constitutes one of the greatest challenges for computational sciences, because of the difficulty to evaluate such systems [1]. Many attempts using various techniques have been developed but no general solution to overcome the sign problem has been found so far [2]. On the other hand, the sign problem appears in important problems in physics. For example, in high energy physics, the sign problem prevents to fully understand the physics of the early universe and to explain and interpret heavy ion collisions. In order to progress with these questions, simulations within the framework of lattice QCD with a non-zero chemical potential would be required. However, these are impossible with present techniques; see refs. [3, 4] for recent reviews. The reason is that standard computations in lattice QCD employ Markov Chain Monte Carlo (MC-MC) methods which need a positiv integrand in order to be applicable. However, in the problem just mentioned a chemical potential is required leading to a complex integrand and therefore to an oscillating function. In particular, if the sign cancellation errors due to the plural oscillations are of significantly higher magnitude than the real integral value, it becomes unfeasible to evaluate such systems.

Therefore, alternative approaches to MC-MC methods need to be developed and in [5, 6] we have proposed and tested Quasi Monte Carlo and iterated numerical integration techniques. These methods can improve the convergence of the involved integrations and also have the potential to deal with the sign problem. However, in this paper we discuss yet another method of numerical integration for generic systems with a sign problem. This new method leads to an arbitrarily precise evaluation of the involved integrals and is based on a *complete symmetrization* of the integrals considered.

This can be achieved through new integration rules on compact groups, as developed in this article, which lead to polynomial exactness. We test the method on the example of 1-dimensional QCD with a chemical potential, see e.g. [7], for which already other approaches have been used to solve the sign problem [8]. Although 1-dimensional QCD is a model with an interest in its own as the strong coupling limit of QCD [9], we consider it here only as a benchmark model for testing our approach, especially since it is possible to compute observables analytically and, thus, check the numerical results directly. In particular, we will compute the chiral condensate for a broad range of action parameters, including

Email addresses: andreas.ammon@desy.de (A. Ammon), tobias.hartung@kcl.ac.uk (T. Hartung), karl.jansen@desy.de (K. Jansen), leovey@math.hu-berlin.de (H. Leövey), julia.volmer@desy.de (J. Volmer)

values of the chemical potential that are impossible (for all practical purposes) to address with standard Monte Carlo techniques.

The idea to symmetrize the involved integrals in a MC-MC simulation to achieve positivity and stable results has also been proposed in refs. [10, 11]. However, in these works only an incomplete symmetrization has been used and still a large number of Monte Carlo samples were necessary to obtain accurate results. In our approach, we perform a polynomially exact integration avoiding the MC-MC step. This way, we only need a very small number of integration points. In fact, we can reach arbitrary (up to machine) precision for the targeted physical observables and avoid the MC error completely.

For our computations, we employ the compact groups $U(N)$ and $SU(N)$ and give a description for a complete symmetrization for $N \leq 3$. As we will demonstrate, for these cases with our new approach the sign problem is completely avoided.

This paper is composed in the following way: In section 2, we introduce the model of 1-dimensional QCD, show analytic results of the partition function Z, and demonstrate the difficulty to compute Z for specific parameters numerically. In section 3, we describe the polynomially exact method based on completely symmetrized spherical quadrature rules [12]. In section 4, we explain our numerical computations in more detail, show results for the partition function and the chiral condensate, and explain their behavior for different parameter values. In section 5, we finally conclude this paper.

2. One dimensional lattice QCD

Let us consider the following Dirac operator (cf., e.g., [7]) for a lattice with n points

$$\mathfrak{D}(U) = \begin{pmatrix} m & \frac{e^{\mu}}{2}U_1 & & & & \frac{e^{-\mu}}{2}U_n^* \\ -\frac{e^{-\mu}}{2}U_1^* & m & \frac{e^{\mu}}{2}U_2 & & & \\ & -\frac{e^{-\mu}}{2}U_2^* & m & \frac{e^{\mu}}{2}U_3 & & \\ & & \ddots & \ddots & \ddots & \\ & & & -\frac{e^{-\mu}}{2}U_{n-2}^* & m & \frac{e^{-\mu}}{2}U_{n-1} \\ -\frac{e^{\mu}}{2}U_n & & & & -\frac{e^{-\mu}}{2}U_{n-1}^* & m \end{pmatrix} \tag{1}$$

where all empty entries are zero and the corresponding one flavor partition function

$$Z(m, \mu, G, n) = \int_{G^n} \det \mathfrak{D}(U)\ dh_G^n(U) \tag{2}$$

where $G = U(N)$ or $G = SU(N)$, $N \in \mathbb{N}$, and h_G is the corresponding (normalized) Haar measure on G.

In order to reduce the numerical effort in calculating $\det \mathfrak{D}$, we will first reduce the dimension using the following theorem.

Theorem 2.1. *Let* $U_0 := U_n$, $\tilde{m}_1 := m$,

$$\forall j \in [2, n-1] \cap \mathbb{N} : \ \tilde{m}_j := m + \frac{1}{4\tilde{m}_{j-1}}, \tag{3}$$

and

$$\tilde{m}_n := m + \frac{1}{4\tilde{m}_{n-1}} + \sum_{j=1}^{n-1} \frac{(-1)^{j+1}2^{-2j}}{\tilde{m}_j \prod_{k=1}^{j-1} \tilde{m}_k^2}. \tag{4}$$

Then,

$$\det \mathfrak{D} = \det \left(\prod_{j=1}^{n} \tilde{m}_j + 2^{-n}e^{-n\mu} \left(\prod_{j=0}^{n-1} U_j \right)^* + (-1)^n 2^{-n} e^{n\mu} \prod_{j=0}^{n-1} U_j \right). \tag{5}$$

Proof appendix A

□

Remark In particular, in the gauge satisfying $U_j = 1$ except for $U_n = U$, Theorem 2.1 yields

$$\det \mathfrak{D} = \det \left(\prod_{j=1}^{n} \tilde{m}_j + 2^{-n} e^{-n\mu} U^* + (-1)^n 2^{-n} e^{n\mu} U \right) = \det \left(c_1 + c_2 U^* + c_3 U \right), \tag{6}$$

with $c_1 := \prod_{j=1}^{n} \tilde{m}_j$, $c_2 = 2^{-n} e^{-n\mu}$, and $c_3 = (-1)^n 2^{-n} e^{n\mu}$.

Mathematically speaking, (6) is an application of "Fubini"[1] and translation invariance of the Haar measure since $\det \mathfrak{D}$ only depends on $\prod_{j=0}^{n-1} U_j$. We will frequently assume this form of $\mathfrak{D}$ in analytic computations and we have implemented this form of $\mathfrak{D}$ in order to reduce computational overhead. Similarly, c_1, c_2, and c_3 are standard notations in this paper. Since $U \in U(N)$ or $U \in SU(N)$ $\det \mathfrak{D}$ is a polynomial of degree N.

□

As an observable of the model we, investigate the chiral condensate

$$\chi(m, \mu, G, n) = \partial_m \ln Z(m, \mu, G, n) = \frac{\partial_m Z(m, \mu, G, n)}{Z(m, \mu, G, n)} = \frac{\int_G \partial_m \det \mathfrak{D} \; dh_G}{\int_G \det \mathfrak{D} \; dh_G}. \tag{7}$$

Since $\det \mathfrak{D}$ is a polynomial of degree N and the derivative ∂_m only acts on the term $\prod_{j=1}^{n} \tilde{m}_j$ in Theorem 2.1, $\partial_m \det \mathfrak{D}$ is still a polynomial of degree N and $\partial_m \prod_{j=1}^{n} \tilde{m}_j$ can be computed using symbolic differentiation.

Theorem 2.1 not only allows us to reduce numerical overhead but we can furthermore calculate the partition function (2) (and therefore also the chiral condensate) analytically.

Theorem 2.2. *Let $c_1 := \prod_{j=1}^{n} \tilde{m}_j$, $c_2 = 2^{-n} e^{-n\mu}$, and $c_3 = (-1)^n 2^{-n} e^{n\mu}$ with $\tilde{m}_j$ as in Theorem 2.1. Then,*

$$Z(m, \mu, U(1), n) = \int_{U(1)} \det \mathfrak{D}(U) \; dh_{U(1)}(U) = c_1, \tag{8}$$

$$Z(m, \mu, U(2), n) = \int_{U(2)} \det \mathfrak{D}(U) \; dh_{U(2)}(U) = c_1^2 - c_2 c_3, \tag{9}$$

$$Z(m, \mu, SU(2), n) = \int_{SU(2)} \det \mathfrak{D}(U) \; dh_{SU(2)}(U) = c_1^2 + c_2^2 - c_2 c_3 + c_3^2, \tag{10}$$

$$Z(m, \mu, U(3), n) = \int_{U(3)} \det \mathfrak{D}(U) \; dh_{U(3)}(U) = c_1^3 - 2 c_1 c_2 c_3, \tag{11}$$

and

$$Z(m, \mu, SU(3), n) = \int_{SU(3)} \det \mathfrak{D}(U) \; dh_{SU(3)}(U) = c_1^3 - 2 c_1 c_2 c_3 + c_2^3 + c_3^3. \tag{12}$$

Proof appendix B

□

In addition, we can deduce the behavior of Z for $m \searrow 0$.

Corollary 2.3. *Let $\tilde{m}_1 := m$, $\tilde{m}_j := m + \frac{1}{4\tilde{m}_{j-1}}$, $\tilde{m}_n := m + \frac{1}{4\tilde{m}_{n-1}} + \sum_{j=1}^{n-1} \frac{(-1)^{j+1} 4^{-j}}{m \prod_{k=1}^{j-1} \tilde{m}_k \tilde{m}_{k+1}}$, and $c_1 := \prod_{j=1}^{n} \tilde{m}_j$. Then,*

$$\lim_{m \searrow 0} c_1 = \begin{cases} 2^{1-n} & , \; n \in 2\mathbb{N} \\ 0 & , \; n \in 2\mathbb{N} - 1 \end{cases}. \tag{13}$$

[1] Since all our groups are compact, they are unimodular and the Haar measures satisfy $h_{G \times H} = h_G \times h_H$ and $h_{G \rtimes H} = h_G \times h_H$ (cf., e.g., exercise 2.1.7 in [13]).

In particular,

$$\lim_{m\searrow 0} Z(m,\mu,U(1),n) = \begin{cases} 2^{1-n} & , \ n \in 2\mathbb{N} \\ 0 & , \ n \in 2\mathbb{N}-1 \end{cases}, \tag{14}$$

$$\lim_{m\searrow 0} Z(m,\mu,U(2),n) = \begin{cases} 3\cdot 2^{-2n} & , \ n \in 2\mathbb{N} \\ -2^{-2n} & , \ n \in 2\mathbb{N}-1 \end{cases}, \tag{15}$$

$$\lim_{m\searrow 0} Z(m,\mu,SU(2),n) = \begin{cases} 3\cdot 2^{-2n} + 2^{1-2n}\cosh(2n\mu) & , \ n \in 2\mathbb{N} \\ 2^{1-2n}\sinh(2n\mu) - 2^{-2n} & , \ n \in 2\mathbb{N}-1 \end{cases}, \tag{16}$$

$$\lim_{m\searrow 0} Z(m,\mu,U(3),n) = \begin{cases} 4\cdot 2^{-3n} & , \ n \in 2\mathbb{N} \\ 0 & , \ n \in 2\mathbb{N}-1 \end{cases}, \tag{17}$$

$$\lim_{m\searrow 0} Z(m,\mu,SU(3),n) = \begin{cases} 4\cdot 2^{-3n} + 2^{1-3n}\cosh(3n\mu) & , \ n \in 2\mathbb{N} \\ 2^{1-3n}\sinh(3n\mu) & , \ n \in 2\mathbb{N}-1 \end{cases}. \tag{18}$$

Proof appendix C

□

If $n\mu$ is large and m small, we can see clearly why the integrals in Theorem 2.2 are difficult to treat numerically; especially the $U(N)$ cases. If we assume a stochastic approach, e.g., a Monte Carlo method, then each evaluation of $\det \mathfrak{D}$ in the form (6) is a value in the vicinity of $|c_2|^N + |c_3|^N \approx |c_3|^N = 2^{-Nn}e^{Nn\mu}$.[2] However, performing the integration (or taking the limit of infinitely many samples), there is a very high degree of cancellations to be observed. Since discrete Markov Chain Monte Carlo methods perform poorly with respect to such cancellations, they have to overcome an initial error in the vicinity of $e^{Nn\mu}$. In other words, as $n\mu$ grows larger, we need very good algorithms to suppress the initial error and the convergence

$$\text{error} \approx \frac{\text{constant}}{\sqrt{\text{sample size}}}$$

of Monte Carlo methods is simply not viable anymore. For example, in Figure 1, we compare a Monte Carlo method (using re-weighting) to our new, polynomially exact method proposed in section 3 (details of the numerical tests can be found in section 4). The error bars, the known rate of convergence $\frac{1}{\sqrt{\text{sample size}}}$, and the here seen relative error of order 1 show that the Monte Carlo method cannot reach the same level of precision with a reasonable number of samples (note the different scales for the Monte Carlo and polynomially exact results).

3. Efficient quadrature rules over the compact groups

Consider $Z(m,\mu,U(1),n)$ for the moment. As we have mentioned before, the problem is that the integral $\int_{U(1)}(-1)^n 2^{-n}e^{n\mu}U \, dh_{U(1)}(U)$ in (8) vanishes but the modulus of each evaluation $|(-1)^n 2^{-n}e^{n\mu}U|$ is large. However, if we were also to evaluate at $-U$ (or, more generally at t equally spaced points along the unit circle), the two terms would cancel. However, the (geometric) idea of taking opposite points or equally spaced points on circles, is not easy to formalize for $SU(N)$ and $U(N)$ with $N \geq 2$. Instead, we should note that the quadrature rule

$$\int_{U(1)} f(U)dh_{U(1)}(U) \approx \frac{1}{t+1}\sum_{k=1}^{t+1} f\left(e^{\frac{2\pi ik}{t+1}}\right) \tag{19}$$

is a spherical t-design (i.e., an equal weights quadrature rule with spherical polynomial degree of exactness t; cf., Example 5.14 in [14]). Since $\det \mathfrak{D}$ is a polynomial of degree N over the matrix entries for $U(N)$ and $SU(N)$, it suffices to consider t-designs or "weighted" t-designs (polynomially exact rules with possibly non-equal weights) with $t = N$.

[2] $|c_2|^N + |c_3|^N = 2^{-Nn}e^{-Nn\mu} + |(-1)^{Nn}|2^{-Nn}e^{Nn\mu} \approx 2^{-Nn}e^{Nn\mu} = |c_3|^N$, due to the fact that $e^x > e^{-x}$ for $x \in \mathbb{R}_{>0}$ and the (anti)symmetric shape of $e^x \pm e^{-x}$.

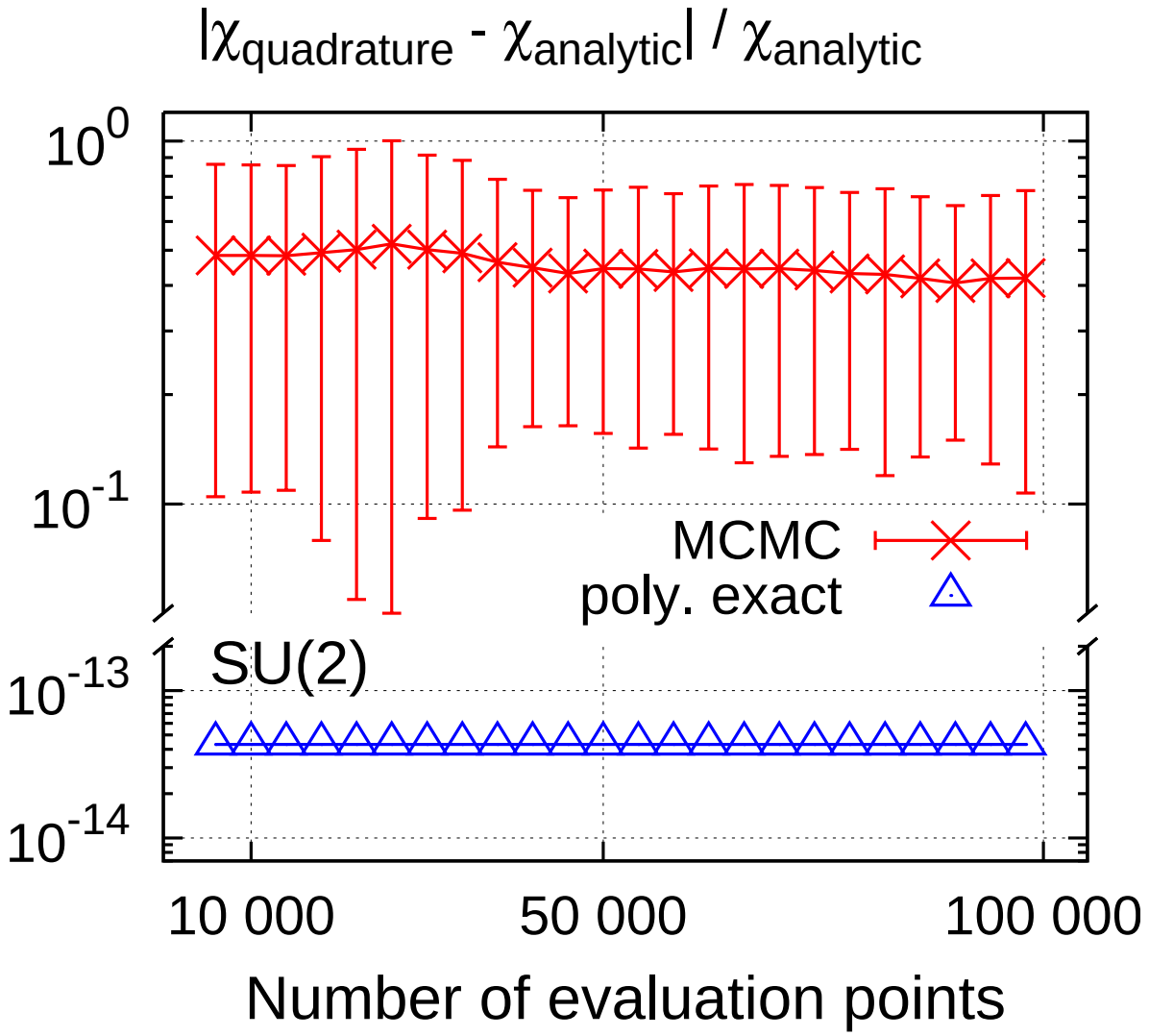

Figure 1: Failure of MC-MC methods. Comparison of the relative error of the chiral condensate χ using polynomially exact (bottom) and Monte Carlo (top) quadrature rules for $SU(2)$. The polynomially exact rule used $n = 8$ integration points, $m = 0.25$, $\mu = 1.0$, and the error bars have been computed from 20 independent repetitions.

In this section, we will discuss the construction of weighted t-designs for $N > 1$ and, especially, why we base the $U(N)$ and $SU(N)$ quadrature on the quadrature rules [12] for the spheres S^N.

Since

$$U(N) \cong SU(N) \rtimes U(1), \tag{20}$$

holds, where $\rtimes$ denotes the (outer) semi-direct product, we may construct a (weighted) t-design $Q_{U(N)}$ over $U(N)$ by considering two different (weighted) t-design rules $Q_{SU(N)}$ and $Q_{U(1)}$ over $SU(N)$ and $U(1)$ correspondingly, and then define the product rule $Q_{U(N)} = Q_{SU(N)} \times Q_{U(1)}$. It is clear that by defining $Q_{U(N)}$ as a product rule in this way, we obtain a (weighted) t-design over $U(N)$. Since t-designs over $U(1)$ are easy to construct (see (19)), the entire problem of constructing (weighted) t-designs for the compact groups considered here reduces to the one of constructing (weighted) t-designs over $SU(N)$.

Starting with $SU(2)$, we have a measure preserving diffeomorphism $SU(2) \cong S^3$. An explicit mapping can be given by

$$\Phi : \ \mathbb{C}^2 \to \mathbb{C}^{2,2}; \ (\alpha, \beta) \mapsto \begin{pmatrix} \alpha & -\beta^* \\ \beta & \alpha^* \end{pmatrix} \tag{21}$$

whose restriction $\Phi|_{S^3}^{SU(2)} : \ S^3 \to SU(2)$ is the mentioned measure preserving diffeomorphism. Thus, for this case we can resort to already well known (weighted) t-designs over the 3-sphere (see [15, 12]) for obtaining (weighted) t-designs over $SU(2)$ trough the mapping Φ.

Moving on to $SU(3)$, we note that there is a correspondence[3] between $SU(3)$ and $S^5 \times SU(2)$. More specifically, we consider first the covering $\Phi_1 : [0, 2\pi)^3 \times [0, \frac{\pi}{2})^2 \to S^5$ defined by

$$\begin{aligned} x_1 &= \cos(\alpha_1)\sin(\varphi_1) \\ x_2 &= \sin(\alpha_1)\sin(\varphi_1) \\ x_3 &= \sin(\alpha_2)\cos(\varphi_1)\sin(\varphi_2) \\ x_4 &= \cos(\alpha_2)\cos(\varphi_1)\sin(\varphi_2) \\ x_5 &= \sin(\alpha_3)\cos(\varphi_1)\cos(\varphi_2) \\ x_6 &= \cos(\alpha_3)\cos(\varphi_1)\cos(\varphi_2) \end{aligned}$$

and note that the restriction $\Phi_1 : [0, 2\pi)^3 \times (0, \frac{\pi}{2})^2 \to S_1^5$, $S_1^5 := \Phi_1\left[[0, 2\pi)^3 \times (0, \frac{\pi}{2})^2\right]$, is a diffeomorphism. Furthermore, the set $S_0^5 := S^5 \setminus S_1^5$ is a null set. On the other hand, we have the mapping $\Phi_2 : \left([0, 2\pi)^3 \times [0, \frac{\pi}{2})^2\right) \times SU(2) \to SU(3)$ defined by

$$\Phi_2((\alpha, \varphi), U) = \begin{pmatrix} e^{i\alpha_1}\cos(\varphi_1) & 0 & e^{i\alpha_1}\sin(\varphi_1) \\ -e^{i\alpha_2}\sin(\varphi_1)\sin(\varphi_2) & e^{-i\alpha_1 - i\alpha_3}\cos(\varphi_2) & e^{i\alpha_2}\cos(\varphi_1)\sin(\varphi_2) \\ -e^{i\alpha_3}\sin(\varphi_1)\cos(\varphi_2) & -e^{-i\alpha_1 - i\alpha_2}\sin(\varphi_2) & e^{i\alpha_3}\cos(\varphi_1)\cos(\varphi_2) \end{pmatrix} \begin{pmatrix} U & 0 \\ 0 & 1 \end{pmatrix}, \quad (22)$$

whose restriction $\Phi_2 : \left([0, 2\pi)^3 \times (0, \frac{\pi}{2})^2\right) \times SU(2) \to SU(3)_1$ with

$$SU(3)_1 := \Phi_2\left[\left([0, 2\pi)^3 \times (0, \frac{\pi}{2})^2\right) \times SU(2)\right], \quad (23)$$

is a bijection and the set $SU(3)_0 := SU(3) \setminus SU(3)_1$ is a Haar null set. Thus, starting with a (weighted) t-design rule Q_{S^3} over S^3 and a (weighted) t-design $Q_{S_1^5}$ over S^5, such that each point of $Q_{S_1^5}$ lies in S_1^5, and considering the mapping

$$\Phi_3 : \ S_1^5 \times S^3 \to SU(3); \ (x, y) := \Phi_2(\Phi_1^{-1}(x), \Phi(y)), \quad (24)$$

we obtain a quadrature rule $Q_{SU(3)}$ over $SU(3)$ by setting $Q_{SU(3)} := \Phi_3\left[Q_{S_1^5} \times Q_{S^3}\right]$.

In fact, by considering (randomized) fully symmetric interpolatory rules $Q^{(1,3)}$ and $Q^{(1,5)}$ from [12] as weighted t-designs Q_{S^3} and $Q_{S_1^5}$, we checked numerically that the resulting quadrature rule $Q_{SU(3)}$ is again a weighted t-design over $SU(3)$, for $t \leq 3$. The latter observation drove us to investigate a procedure more in detail for constructing weighted t-design rules over $SU(N)$, for arbitrary positive integers N and t. This procedure is based on a generalization of the mapping Φ_3 as stated above and relies on the correspondence[4] between $SU(N)$ and $\bigtimes_{j=1}^{N-1} S^{2j+1}$. This new construction of quadrature rules over $SU(N)$ is subject of current research by the authors, but the potential applications of this new method exceed the scope of this article and will be not reported at this point.

4. Numerical results

In this section we will provide a comparison of the evaluation of the partition function Z and the chiral condensate χ using MC-MC and our new polynomially exact integration rules. First we will concentrate on the partition function Z. We will have a short loook at the behavior of the analytic values of Z before comparing them to the quadrature results of Z using the Monte Carlo and polynomially exact method in terms of a relative error. To present the real power of the polynomially exact method, we will show computational results for two different floating point number precisions. Then we will investigate the relative error behavior of the chiral condensate. Since we compute the relative error as the deviation of the quadrature result from the computation using analytic formulae, we explicitly differentiate these ways of computation in the following using the terms $Z_{\text{quadrature}}$ and Z_{analytic}.

As stated above, for the here considered model both, Z and χ can be computed analytically for the groups $U(N)$ and $SU(N)$. In particular, the expression of the partition functions in Theorem 2.2 for

[3] More precisely, $SU(N)$ is a principal $SU(N-1)$ bundle over S^{2N-1}; cf., e.g., [16, equation (22.18)].

[4] Induction over $SU(j)$ being a principal $SU(j-1)$ bundle over S^{2j-1} [16, equation (22.18)] and $SU(2) \cong S^3$.

$SU(N)$ can be related to the one for $U(N)$ through

$$\begin{aligned} Z_{\text{analytic}}(m,\mu,SU(N),n) =& Z_{\text{analytic}}(m,\mu,U(N),n) + c_2^N + c_3^N \\ =& Z_{\text{analytic}}(m,\mu,U(N),n) + \begin{cases} 2^{1-Nn}\cosh(Nn\mu) & ,\ n \in 2\mathbb{N} \\ -2^{1-Nn}\sinh(Nn\mu) & ,\ n \in 2\mathbb{N}-1\ . \end{cases} \end{aligned} \tag{25}$$

We note that for $U(N)$ the partition function smoothly approaches a much smaller value than $c_2^N + c_3^N$ when decreasing the mass parameter m while for $SU(N)$ it approaches a constant near $c_2^N + c_3^N$ as given in Theorem 2.2, see also Corollary 2.3. The behavior of $Z_{\text{analytic}}(m,\mu,G,n)$ as a function of the mass parameter m for $G \in \{U(3), SU(3)\}$, $n = 6$, $\mu = 1$, is shown in Figure 2 and there we can clearly see the different behaviors of Z_{analytic} for $U(3)$ and $SU(3)$ for $m \searrow 0$.

For the groups $U(N)$ and $SU(N)$ each point evaluation of the quadrature rule is of order $O(2^{-Nn}e^{Nn\mu})$, that is, a double precision computation cannot resolve values below $10^{-16}2^{-Nn}e^{Nn\mu}$. Since the behavior of the partition function in comparison to the constant $c_2^N + c_3^N$ will be important in order to understand the relative error $|Z_{\text{quadrature}} - Z_{\text{analytic}}|/Z_{\text{analytic}}$, we also show the value of $|c_2^3 + c_3^3| \approx 2^{-3n}e^{3n\mu}$ in Figure 2 (see discussion at the end of section 2 above, as well) for the examples of $U(3)$ and $SU(3)$. In Figure 2, we furthermore distinguished three regions with different behavior, indicated in the following by region I, II and III.

Let us first discuss the group $U(3)$. For large values of m (region III) $2^{-3n}e^{3n\mu}$ is negligible compared to Z_{analytic}. We therefore expect a small deviation of $Z_{\text{quadrature}}$ from Z_{analytic} and hence a small relative error. On the other hand, for small values of m (region I) Z_{analytic} becomes much smaller than $2^{-3n}e^{3n\mu}$ and we expect a significant relative error due to rounding errors. There is also a transition regime in m (region II) in which the values of Z_{analytic} and $2^{-3n}e^{3n\mu}$ have the same order of magnitude. Hence, we expect a significant increase in the relative error while decreasing m, but the smooth behavior of Z_{analytic} for $U(3)$ suggests that there will be a similarly smooth increase of the relative error as a function of m. As we will discuss below, this expectation is indeed verified in our numerical tests.

In the $SU(3)$ case, we have the additional constant $c_2^3 + c_3^3$ which, for m small, is significantly larger than $Z_{\text{analytic}}(U(3))$, see (25). Looking at Figure 2, we expect a relative error similar to the $U(3)$ case in region III. In region I, though, the relative error should be much less now due to the fact that the analytic value and order of magnitude of each point evaluation are closer together than in the $U(3)$ case. In the transition region II, the behavior may be different to $U(3)$ as well, although this is not deduced from the figure per se but from the differences in the formulae of Z_{analytic} (25). There, the m-dependent term of Z_{analytic}, the constant $c_2^N + c_3^N$, and the point evaluation in the quadrature rules are of the same order of magnitude $O(2^{-Nn}e^{Nn\mu})$. Thus, this additional term $c_2^N + c_3^N$, not present at $U(N)$, could lead to competing effects for the relative error and, hence, an irregular behavior of the relative error (at least in the MC-MC case).

Let us now move on to our numerical experiments. In Figure 3, we compare the quadrature rule

$$Z^{\text{MCMC}}_{\text{quadrature}}(m,\mu,G,n) = \int_G \det \mathfrak{D}\ dh_G \approx \frac{1}{\#Q_G}\sum_{k=1}^{\#Q_G} \det \mathfrak{D}(U_k) \tag{26}$$

where each U_k is chosen randomly in G (uniformly with respect to the Haar measure) and the polynomially exact version

$$Z^{\text{poly. exact}}_{\text{quadrature}}(m,\mu,G,n) = \int_G \det \mathfrak{D}\ dh_G \approx \frac{1}{\#Q_G}\sum_{V\in Q_G} \det \mathfrak{D}(VU_1) \tag{27}$$

where U_1 is the U_1 sampled in the non-exact version in (26).[5] Here, we chose

$$Q_G = \begin{cases} \left\{ e^{\frac{2\pi i k}{4}};\ k \in \mathbb{Z}_4 \right\} & ;\ G = U(1) \\ \Phi\left[Q_{S^3}\right] & ;\ G = SU(2) \\ \left\{ e^{\frac{2\pi i k}{4}}U;\ k \in \mathbb{Z}_4,\ U \in \Phi\left[Q_{S^3}\right] \right\} & ;\ G = U(2) \\ \Phi_3\left[Q_{S^5_1} \times Q_{S^3}\right] & ;\ G = SU(3) \\ \left\{ e^{\frac{2\pi i k}{4}}U;\ k \in \mathbb{Z}_4,\ U \in \Phi_3\left[Q_{S^5_1} \times Q_{S^3}\right] \right\} & ;\ G = U(3) \end{cases} \tag{28}$$

[5] Any $U_1 \in G$ would be perfectly fine; in fact, choosing the identity for U_1 would be a good canonical choice. However, we chose U_1 randomly (uniformly with respect to the Haar measure) in order to approximate the error.

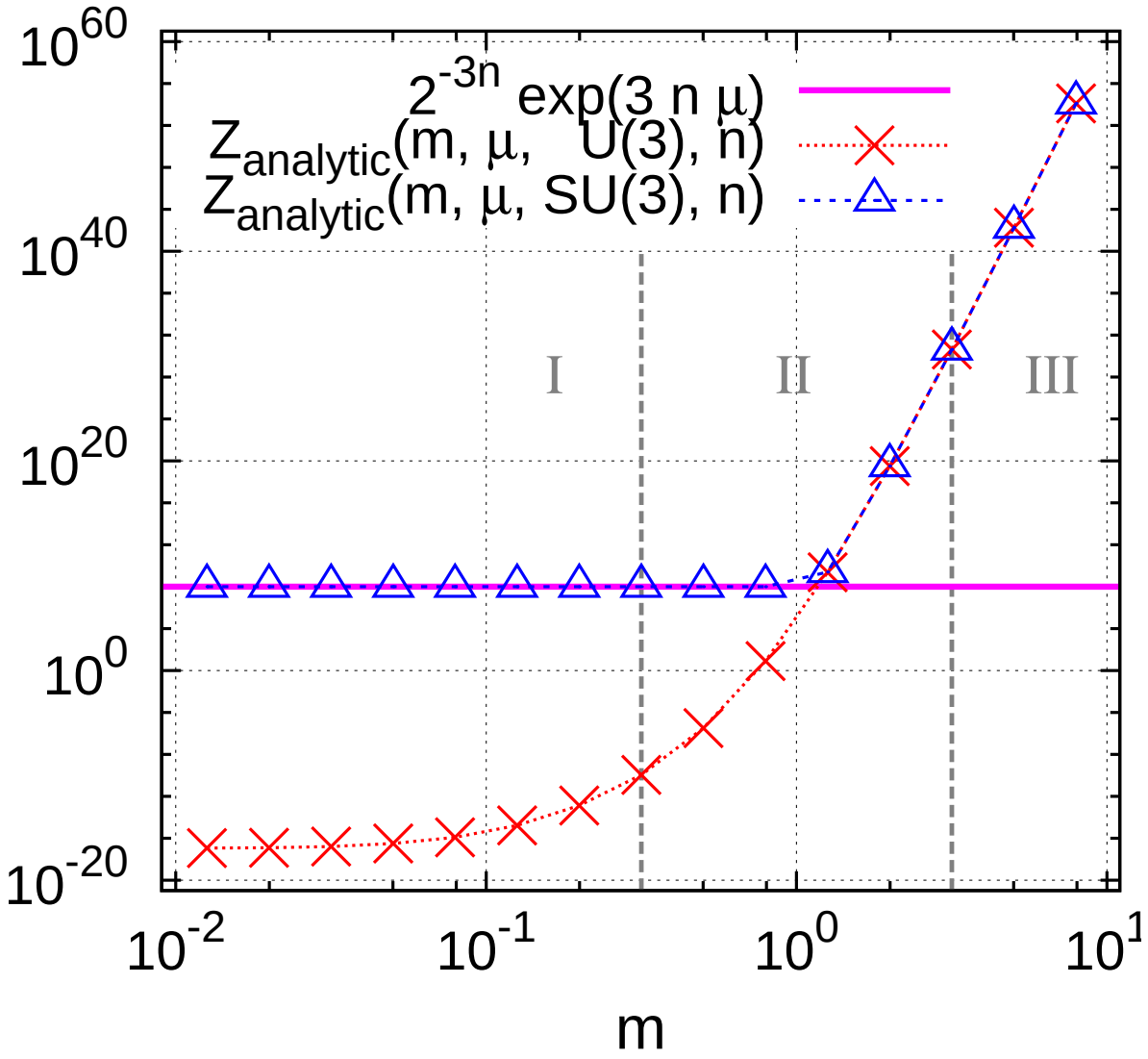

Figure 2: Order of the quadrature rule point evaluation of the partition function integrand, $\left(2^{-n}e^{n\mu}\right)^3$, see (6), compared to the analytic values of the partition functions for $U(3)$ and $SU(3)$ (see Theorem 2.2), using $n = 20$, $\mu = 1$. As discussed in the paper, the ratio $Z_{\text{analytic}}/2^{-3n}e^{3n\mu}$ determines the relative errors of the partition function and the chiral condensate to a large extent. In particular, we identify three regions (I, II, III) in which the relative error exhibits qualitatively different behavior. (These computations were performed with 1024bit floating point arithmetic.)

where Q_{S^3} and $Q_{S^5_1}$ are randomized fully symmetric rules of polynomial degree 3 on S^3 and S^5 according to [12]. To obtain the error estimates, we repeated each numerical experiment 50 times.

Figure 3 shows the relative error of the partition function computed according to (26) and (27). The same m-regions (I, II, and III), as shown in Figure 2, are indicated here as well and we can see that the behavior of the relative error is quite distinct for each of the three regions. For large values of m (region III), both methods operate with double precision as expected from the discussion above.

Regarding regions I and II, we will consider the $U(N)$ case first. As we move to smaller m, we enter the transition region (II) and for $U(N)$ the relative error increases significantly but in a smooth way. As shown in Figure 2, for very small values of m (region I) $Z_{\text{analytic}}(m, \mu, U(N), n)$ is significantly smaller than $2^{-Nn}e^{Nn\mu}$; hence, $Z_{\text{analytic}}(m, \mu, U(N), n)$ is negligible compared to the machine error and we observe large relative errors in region I of Figure 3. Note that the polynomially exact computation still sums values of magnitude $2^{-Nn}e^{Nn\mu}$, i.e., the relative error of the exact method cannot be below 10^{-16} times the error of the non-exact method which is, indeed, what we see in Figure 3. Returning to Figure 2 and the $U(N)$ discussion above, the observed smooth increase of the relative error in region II matches our expectations.

In the $SU(N)$ case, the relative error is comparable to the $U(N)$ case in regions I and III; we simply obtain smaller errors in region I since $2^{-Nn}e^{Nn\mu}$ does not dominate Z_{analytic} as is the case for $U(N)$.

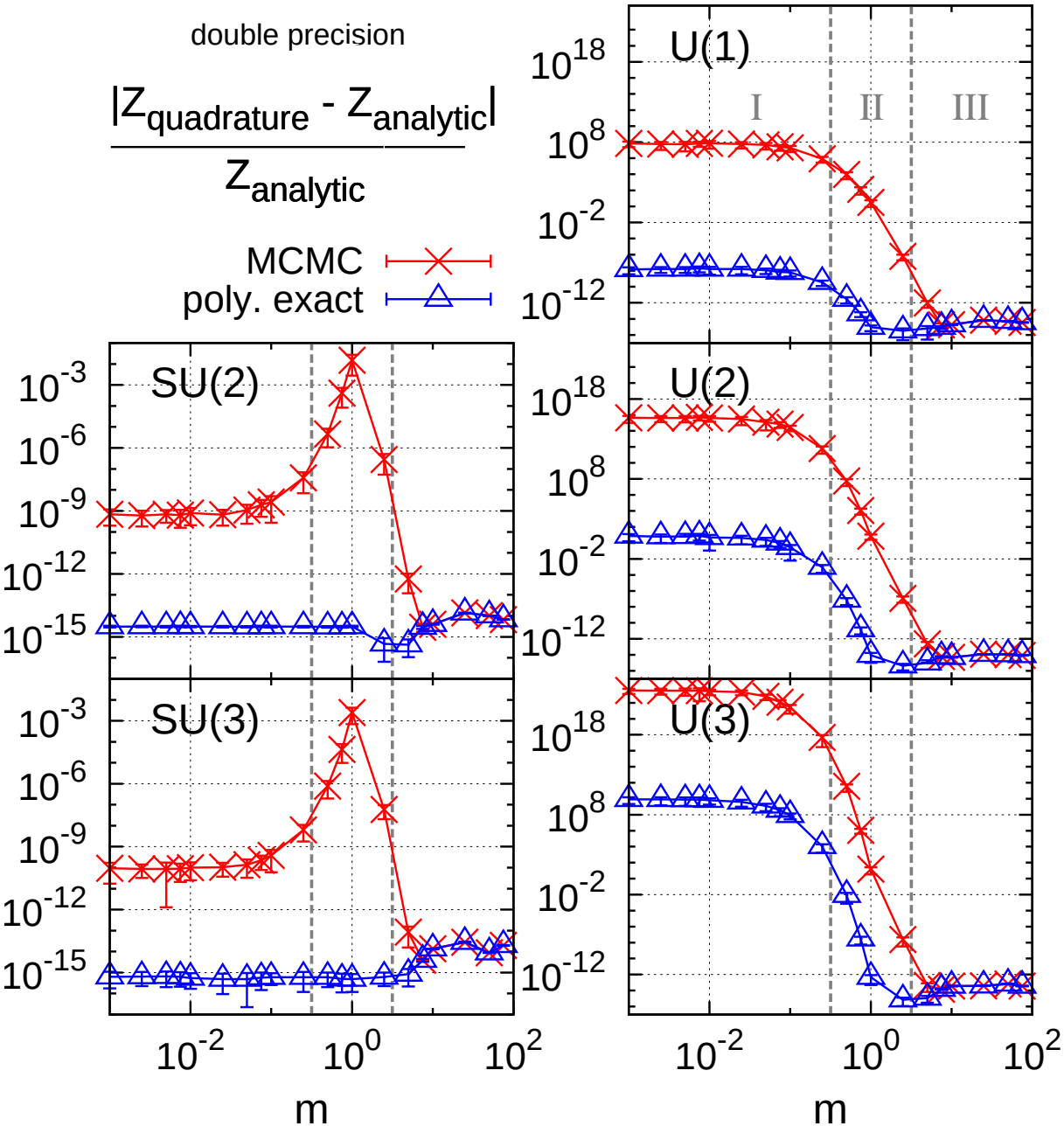

Figure 3: Comparison of the relative error of the used methods, namely the polynomially exact and Monte Carlo quadrature rules to calculate the partition function Z for $SU(2)$ and $SU(3)$ (left column, top to bottom), and $U(1)$, $U(2)$, and $U(3)$ (right column, top to bottom) with $n = 20$, $\mu = 1$, $m \in [0.001, 100]$. Averages and standard deviations (error bars) have been computed from 50 independent computations. Here we used double precision to carry through the numerical calculations. The different behaviors of the relative error regarding different values of m are divided into regions I, II and III, corresponding to Figure 2.

However, in the transition region II of Figure 3, we can see a rather irregular behavior whose possibility to occur we already mentioned in the discussion of Z_{analytic} above. This can be attributed to the fact that the mass dependent term of $Z_{\text{analytic}}(m, \mu, U(N), n)$ and the constant $c_2^N + c_3^N$, see (25), as well as the point evaluations in $Z_{\text{quadrature}}$, are of the same order of magnitude. Hence neither term can suppress the error of the other which we interpret as the cause of the peak in the relative error.

Figure 4 shows the same comparison as Figure 3 but computations were performed with 1024bit floating point arithmetic,[6] i.e., approximately 307 digit precision. Again, we observe that the polynomially exact method operates on machine precision (as to be expected). The averages and standard deviations

[6]These are 1024 mantissa bits; double precision (about 15 digit precision) corresponds to 53bit.

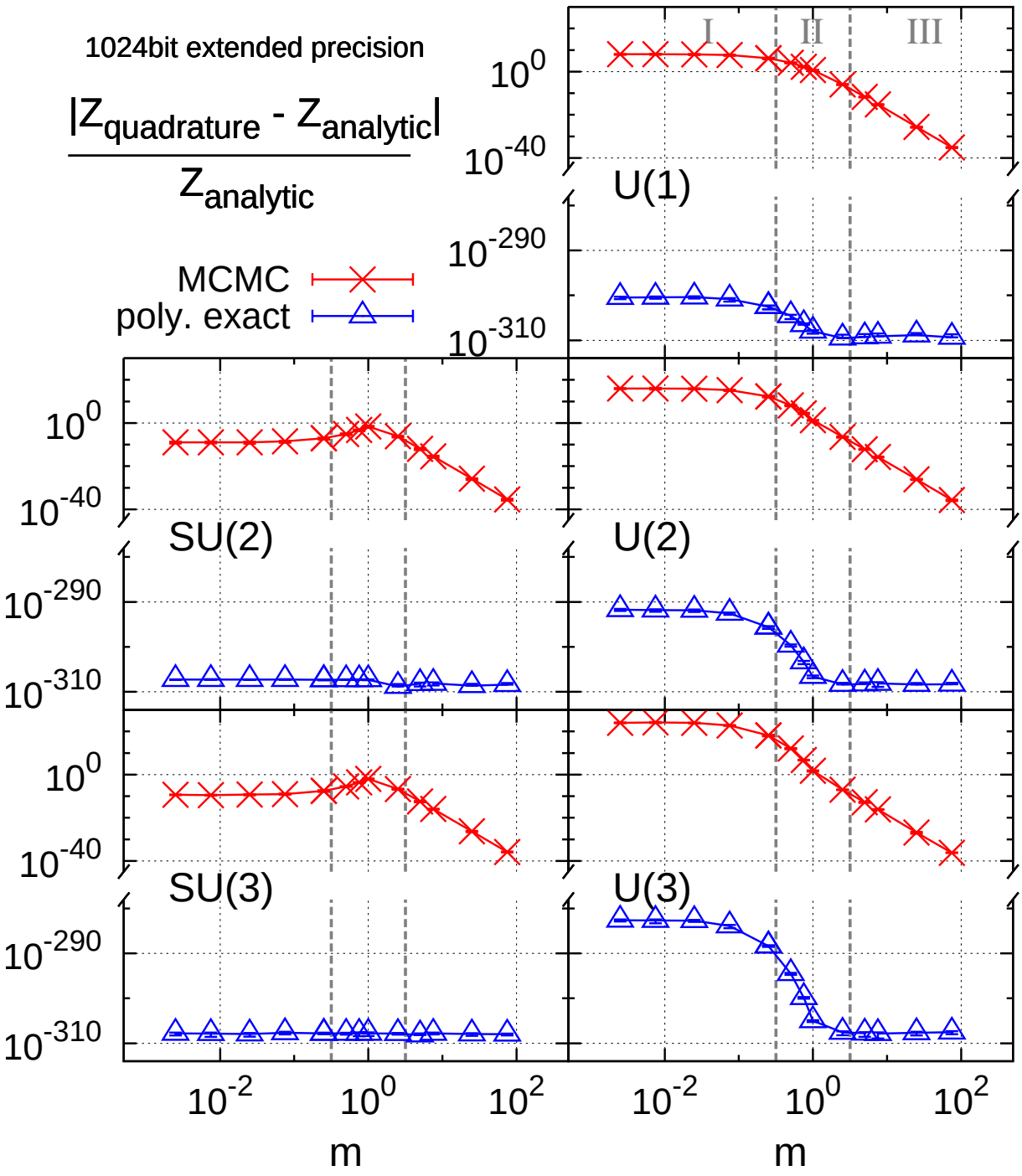

Figure 4: Comparison of the relative error as shown in Figure 3 but here using 1024bit extended floats. Averages and standard deviations (error bars) have been computed from 50 independent computations for $U(1)$, $U(2)$, and $SU(2)$, and from 10 independent computations for $SU(3)$ and $U(3)$. Used are again $n = 20$, $\mu = 1$, $m \in [0.001, 100]$

of the relative error were computed from 50 independent computations for $G \in \{U(1), SU(2), U(2)\}$ and from 10 independent computations for $G \in \{SU(3), U(3)\}$. All computations were performed on an IBM laptop in less than an hour.[7] The behavior of the relative error, for both Monte-Carlo and the polynomially exact method, is very similar to the double precision case in Figure 3. Note that the polynomially exact integration always leads to machine precision results even in this extreme case of 1024bit precision whereas the relative error of the MC-MC results does not notably decrease in regions I and II when replacing double precision floats in Figure 3 with 1024bit extended floats in Figure 4.

[7] Only for $SU(3)$ and $U(3)$, run-time was considerably longer than a few minutes.

In general, we observe in Figure 3 and Figure 4 that the polynomially exact quadrature rule always provides machine error results.

In order to test our new polynomially exact method against an actual physical observable, Figure 5 shows the comparison of the relative error of the chiral condensate (using 1024bit extended floats again). The analytic values of the chiral condensate have been obtained through symbolic differentiation of the formulae in Theorem 2.2; the numerical values by symbolic differentiation of (6). We observe that the relative error follows the trend we have already seen for the partition function in the three different regions.[8]

Let us discuss the relative error in Figure 5 in a bit more detail. A first observation is that the polynomially exact method operates on the level of machine precision and, as such, reduces the relative error by (many) orders of magnitude for all values of m. Even more interesting and striking is but the size of the relative error of the chiral condensate in the small-m region. As pointed out in [7], in this region of parameter space there is a severe sign problem. Indeed, for the MC-MC method the relative error becomes $O(1)$ for sufficiently small m, i.e., no statistically significant result for the chiral condensate can be obtained with standard MC-MC calculations. (In Figure 5, this behavior can only be seen for $U(N)$ but it is also present and was observed by us for $SU(N)$ for m-values smaller than the ones shown here.[9]) This is a clear manifestation of the infamous sign problem.

In contrast, our polynomially exact method provides results on machine precision, again. Thus, the polynomially exact method completely overcomes the sign problem and can lead to very accurate results even in regions where MC-MC computations are unfeasible.

5. Conclusion

In this work, we have developed and tested a new integration method for the groups $U(N)$ and $SU(N)$. As a major outcome of our work, we could in fact provide a numerical verification that the here developed method leads to polynomial exactness of the integration for $N \leq 3$. We have applied the method to the 1-dimensional QCD with a chemical potential where for certain values of the action parameters a sign problem appears with MC-MC methods. Using the groups $U(1), U(2), U(3)$ and $SU(2), SU(3)$ we have demonstrated that even for cases when the sign problem is most severe, the chiral condensate of this model can be computed to arbitrary precision with the new method. In contrast, standard Markov Chain Monte Carlo methods show large $O(1)$ relative errors and do not give any statistically significant result. For this comparison, we even went to 1024bit extended precision and were able to show that our new method still achieves results on the level of machine precision. We, therefore, conclude that our polynomially exact integration method can completely avoid the sign problem. Furthermore, it is important to point out that it also leads to orders of magnitude reduced errors compared to MC-MC even in regions of parameter space where no sign problem occurs.

The fact that our new integration method overcomes the sign problem and leads to orders of magnitude reduced errors in general in the here considered 1-dimensional QCD is certainly a very promising finding and stands as a result by itself. However, this benchmark model can only be regarded as a toy example. It will be necessary to demonstrate that the method can also be applied in higher dimensions. To this end, we are presently considering the Schwinger model as an example of a quantum field theory in 2 dimensions.

Also, so far we do not have proof yet of the polynomial exactness for the groups $U(N)$ and $SU(N)$ with general N. Although we are very confident that our integration method leads to polynomial exactness for general N we are working on a proof to substantiate this statement.

[8] Here, the range of the regions differs from before.

[9] The larger relative error $> O(1)$ for $SU(N)$ at small m seen here is due to $\lim_{m \searrow 0} \chi_{\text{analytic}}(m, \mu, SU(N), n) = 0$, because $\lim_{m \searrow 0} \partial_m Z_{\text{analytic}}(m, \mu, SU(N), n) = 0$ and $\lim_{m \searrow 0} Z_{\text{analytic}}(m, \mu, SU(N), n) \neq 0$. Thus, the analytic result for some small m is already at machine precision while the quadrature result is not, such that division by this small machine precision number yields a value which can be larger than one.

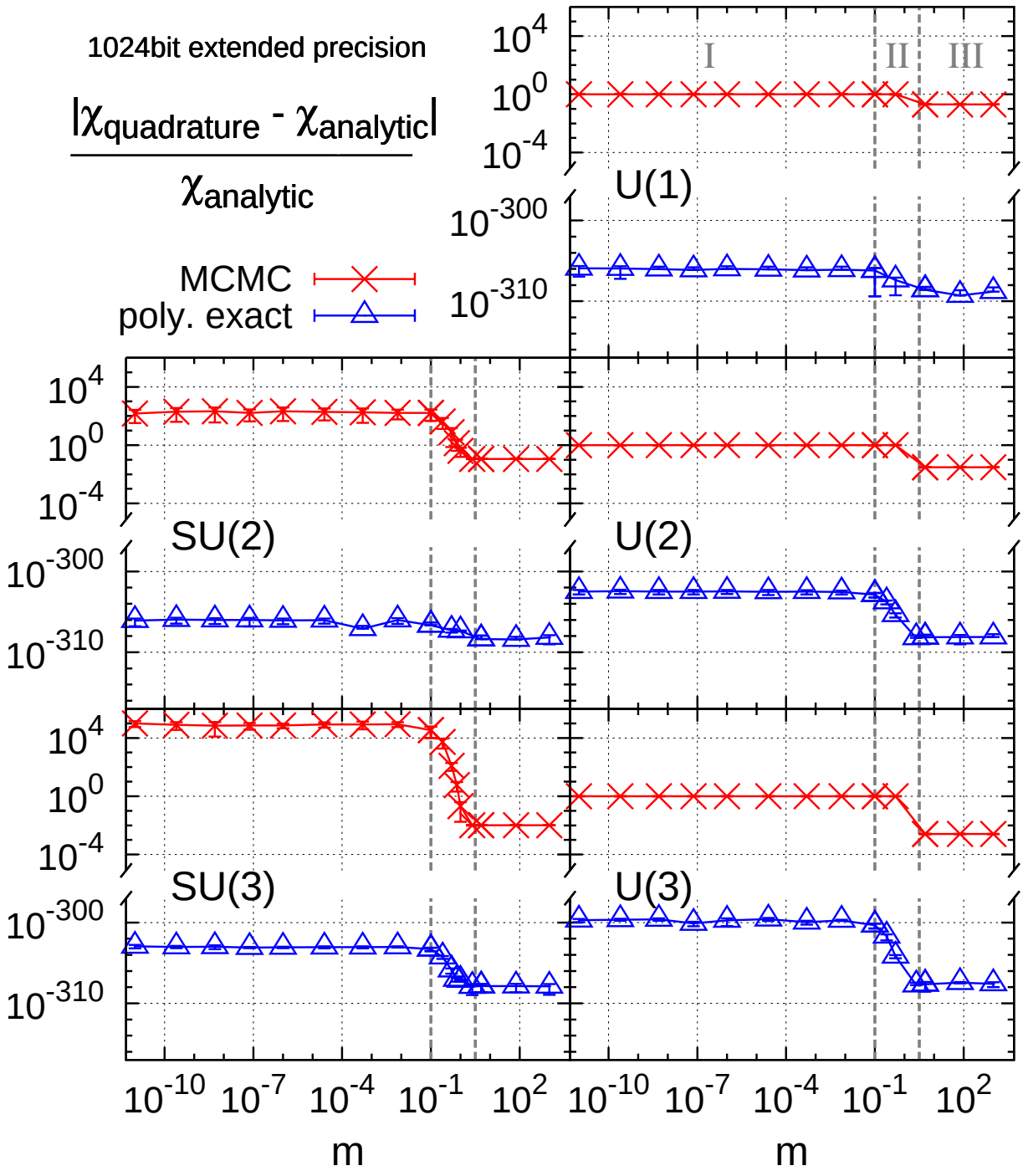

Figure 5: Comparison of the relative error of the chiral condensate $\chi = \partial_m \ln Z$ using polynomially exact and Monte Carlo quadrature rules for $SU(2)$ and $SU(3)$ (left column, top to bottom), and $U(1)$, $U(2)$, and $U(3)$ (right column, top to bottom) with $n = 8$, $\mu = 1.0$, and $m \in [10^{-11}, 10^{3}]$. 1024bit extended floats are used. Averages and standard deviations (error bars) have been computed from 50 independent computations for $SU(2)$, $U(1)$ and $U(2)$ and from 5 for $SU(3)$ and $U(3)$. The different behaviors of the error regarding different values of m are divided into regions I, II and III.

Acknowledgment

The authors wish to express their gratitude to Prof. Andreas Griewank for inspiring comments and conversations, which helped to develop the work in this article. H.L. and J.V. acknowledge financial support by the DFG-funded projects JA 674/6-1 and GR 705/13.

References

[1] Matthias Troyer and Uwe-Jens Wiese. Computational complexity and fundamental limitations to fermionic quantum Monte Carlo simulations. *Phys. Rev. Lett.*, 94:170201, 2005. doi: 10.1103/PhysRevLett.94.170201.

[2] Christof Gattringer and Kurt Langfeld. Approaches to the sign problem in lattice field theory. 2016.

[3] Dénes Sexty. New algorithms for finite density QCD. *PoS*, LATTICE2014:016, 2014.

[4] Christof Gattringer. New developments for dual methods in lattice field theory at non-zero density. *PoS*, LATTICE2013:002, 2014.

[5] K. Jansen, H. Leovey, Andreas Ammon, A. Griewank, and M. Muller-Preussker. Quasi-Monte Carlo methods for lattice systems: a first look. *Comput.Phys.Commun.*, 185:948–959, 2014. doi: 10.1016/j.cpc.2013.10.011.

[6] A. Ammon, A. Genz, T. Hartung, K. Jansen, H. Leövey, and J. Volmer. On the efficient numerical solution of lattice systems with low-order couplings. *Comput. Phys. Commun.*, 198:71–81, 2016. doi: 10.1016/j.cpc.2015.09.004.

[7] L. Ravagli and J. J. M. Verbaarschot. QCD in One Dimension at Nonzero Chemical Potential. *Phys. Rev.*, D76:054506, 2007. doi: 10.1103/PhysRevD.76.054506.

[8] Gert Aarts and K. Splittorff. Degenerate distributions in complex langevin dynamics: one-dimensional qcd at finite chemical potential. *Journal of High Energy Physics*, 2010(8):1–19, 2010. ISSN 1029-8479. doi: 10.1007/JHEP08(2010)017. URL `http://dx.doi.org/10.1007/JHEP08(2010)017`.

[9] Ernst-Michael Ilgenfritz and J. Kripfganz. Dynamical Fermions at Nonzero Chemical Potential and Temperature: Mean Field Approach. *Z. Phys.*, C29:79–82, 1985. doi: 10.1007/BF01571383. [,I.57(1984)].

[10] Jacques Bloch, Falk Bruckmann, and Tilo Wettig. Subset method for one-dimensional QCD. *JHEP*, 10:140, 2013. doi: 10.1007/JHEP10(2013)140.

[11] Jacques Bloch, Falk Bruckmann, and Tilo Wettig. Sign problem and subsets in one-dimensional QCD. *PoS*, LATTICE2013:194, 2014.

[12] A. Genz. Fully Symmetric Interpolatory Rules for Multiple Integrals over Hyper-Spherical Surfaces. *Journal of Computational and Applied Mathematics*, 157:187–195, 2003. doi: 10.1016/S0377-0427(03)00413-8.

[13] H. Abbaspour and M. Moskowitz. *Basic Lie Theory*. World Scientific, 2007.

[14] P. Delsarte, J. M. Goethals, and J. J. Seidel. Spherical Codes and Designs. *Geometriae Dedicata*, 6: 363–388, 1977.

[15] Ian H. Sloan and Robert S. Womersley. Good approximation on the sphere, with application to geodesy and the scattering of sound. *Journal of Computational and Applied Mathematics*, 149(1):227 – 237, 2002. ISSN 0377-0427. doi: http://dx.doi.org/10.1016/S0377-0427(02)00532-0. URL `http://www.sciencedirect.com/science/article/pii/S0377042702005320`. Scientific and Engineering Computations for the 21st Century - Me thodologies and Applications Proceedings of the 15th Toyota Conference.

[16] T. Frankel. *The Geometry of Physics: An Introduction*. Cambridge University Press, 3rd edition edition, 2012.

[17] Christof Gattringer and Christian B. Lang. Quantum chromodynamics on the lattice. *Lect.Notes Phys.*, 788:1–211, 2010. doi: 10.1007/978-3-642-01850-3.

Appendix A: Proof of Theorem 2.1
Let

$$Y = \begin{pmatrix} A & B \\ C & D \end{pmatrix} \tag{.1}$$

be a block decomposition where A and D are square matrices and A is invertible. Then,

$$\det Y = \det A \det \left(D - CA^{-1}B\right). \tag{.2}$$

Here, we are considering matrices of the form

$$X = \begin{pmatrix} m_1 & \frac{e^{\mu}}{2}U_1 & & & & \frac{e^{-\mu}}{2}U_n^* \\ -\frac{e^{-\mu}}{2}U_1^* & m_2 & \frac{e^{\mu}}{2}U_2 & & & \\ & -\frac{e^{-\mu}}{2}U_2^* & m_3 & \frac{e^{\mu}}{2}U_3 & & \\ & & \ddots & \ddots & \ddots & \\ & & & -\frac{e^{-\mu}}{2}U_{n-2}^* & m_{n-1} & \frac{e^{\mu}}{2}U_{n-1} \\ -\frac{e^{\mu}}{2}U_n & & & & -\frac{e^{-\mu}}{2}U_{n-1}^* & m_n \end{pmatrix} \tag{.3}$$

where all m_i are positive. Choosing A to be the m_1 block in X, we obtain

$$D = \begin{pmatrix} m_2 & \frac{e^{\mu}}{2}U_2 & & & & \\ -\frac{e^{-\mu}}{2}U_2^* & m_3 & \frac{e^{\mu}}{2}U_3 & & & \\ & -\frac{e^{-\mu}}{2}U_3^* & m_4 & \frac{e^{\mu}}{2}U_4 & & \\ & & \ddots & \ddots & \ddots & \\ & & & -\frac{e^{-\mu}}{2}U_{n-2}^* & m_{n-1} & \frac{e^{\mu}}{2}U_{n-1} \\ & & & & -\frac{e^{-\mu}}{2}U_{n-1}^* & m_n \end{pmatrix} \tag{.4}$$

and

$$-CA^{-1}B = \frac{-1}{m_1}\begin{pmatrix} -\frac{1}{4} & 0 & -\frac{e^{-2\mu}}{4}U_1^*U_n^* \\ 0 & 0 & 0 \\ -\frac{e^{2\mu}}{4}U_nU_1 & 0 & -\frac{1}{4} \end{pmatrix}. \tag{.5}$$

In other words, $D - CA^{-1}B$ is of the initial form again and

$$\det X = m_1^N \det(D - CA^{-1}B) \tag{.6}$$

$$= \det \begin{pmatrix} m_2 + \frac{1}{4m_1} & \frac{e^{\mu}}{2}U_2 & & & & \frac{2^{-2}e^{-2\mu}}{m_1}U_1^*U_n^* \\ -\frac{e^{-\mu}}{2}U_2^* & m_3 & \frac{e^{\mu}}{2}U_3 & & & \\ & -\frac{e^{-\mu}}{2}U_3^* & m_4 & \frac{e^{\mu}}{2}U_4 & & \\ & & \ddots & \ddots & \ddots & \\ & & & -\frac{e^{-\mu}}{2}U_{n-2}^* & m_{n-1} & \frac{e^{\mu}}{2}U_{n-1} \\ \frac{2^{-2}e^{2\mu}}{m_1}U_nU_1 & & & & -\frac{e^{-\mu}}{2}U_{n-1}^* & m_n + \frac{1}{4m_1} \end{pmatrix}. \tag{.7}$$

Let $U_0 := U_n$, $\tilde{m}_1 := m_1$,

$$\forall j \in [2, n-1] \cap \mathbb{N} : \ \tilde{m}_j := m_j + \frac{1}{4\tilde{m}_{j-1}}, \tag{.8}$$

and

$$\tilde{m}_n := m_n + \frac{1}{4\tilde{m}_{n-1}} + \sum_{j=1}^{n-1} \frac{(-1)^{j+1}2^{-2j}}{\tilde{m}_j \prod_{k=1}^{j-1} \tilde{m}_k^2}. \tag{.9}$$

Then, we obtain inductively

$$\det X \tag{.10}$$

$$= \prod_{j=1}^{n-3} \tilde{m}_j^N \det \begin{pmatrix} \tilde{m}_{n-2} & \frac{e^{\mu}}{2} U_{n-2} & \frac{2^{-(n-2)} e^{-(n-2)\mu}}{\prod_{j=1}^{n-3} \tilde{m}_j} \left(\prod_{j=1}^{n-2} U_{j-1} \right)^* \\ -\frac{e^{-\mu}}{2} U_{n-2}^* & m_{n-1} & \frac{e^{\mu}}{2} U_{n-1} \\ \frac{(-1)^{n-2} 2^{-(n-2)} e^{(n-2)\mu}}{\prod_{j=1}^{n-3} \tilde{m}_j} \prod_{j=1}^{n-2} U_{j-1} & -\frac{e^{-\mu}}{2} U_{n-1}^* & m_n + \sum_{j=1}^{n-3} \frac{(-1)^j 2^{-2j}}{\tilde{m}_j \prod_{k=1}^{j-1} \tilde{m}_k^2} \end{pmatrix} \tag{.11}$$

$$= \prod_{j=1}^{n-1} \tilde{m}_j^N \det \left(\tilde{m}_n + \frac{(-1)^n 2^{-n} e^{n\mu}}{\prod_{j=1}^{n-1} \tilde{m}_j} \prod_{j=1}^{n} U_{j-1} + \frac{2^{-n} e^{-n\mu}}{\prod_{j=1}^{n-1} \tilde{m}_j} \left(\prod_{j=1}^{n} U_{j-1} \right)^* \right) \tag{.12}$$

which finally yields

$$\det X = \det \left(\prod_{j=1}^{n} \tilde{m}_j + (-1)^n 2^{-n} e^{n\mu} \prod_{j=1}^{n} U_{j-1} + 2^{-n} e^{-n\mu} \left(\prod_{j=1}^{n} U_{j-1} \right)^* \right). \tag{.13}$$

Appendix B: Proof of Theorem 2.2

Note that the $U(1)$ case is trivial. Hence, we will start considering $U(N)$ with $N \geq 2$ and use the notations

$$U_{ij}^* := (U^*)_{ij} \tag{.1}$$

and

$$\forall p \in \mathbb{N}_0 \ \forall I, J \in \mathbb{N}_{\leq N}^p : \ U_{IJ} := \prod_{k=0}^{p-1} U_{I_k J_k} \ \wedge \ U_{IJ}^* := \prod_{k=0}^{p-1} (U^*)_{I_k J_k} . \tag{.2}$$

Furthermore, we set $\forall p, q \in \mathbb{N}_0 \ \forall I, J \in \mathbb{N}_{\leq N}^p \ \forall K, L \in \mathbb{N}_{\leq N}^q$:

$$\langle I, J | K, L \rangle := \int_{U(N)} U_{IJ}^* U_{KL} dh_{U(N)}(U) \tag{.3}$$

and use abbreviations for empty sets or singletons similar to

$$\langle 0, 1 | \rangle := \langle (0), (1) | (), () \rangle. \tag{.4}$$

The following identities are well-known (cf., e.g., [17]).

- $p \neq q \ \Rightarrow \ \langle I, J | K, L \rangle = 0$
- $\langle | \rangle = 1$
- $\langle i, j | k, l \rangle = \frac{\delta_{il} \delta_{jk}}{N}$

For $N = 2$, we may expand the determinant in

$$\int_{U(2)} \det \mathfrak{D} \ dh_{U(2)} = \int_{U(2)} \det \left(c_1 + c_2 U^* + c_3 U \right) dh_{U(2)}(U) \tag{.5}$$

$$= \int_{U(2)} \det \begin{pmatrix} c_1 + c_2 U_{00}^* + c_3 U_{00} & c_2 U_{01}^* + c_3 U_{01} \\ c_2 U_{10}^* + c_3 U_{10} & c_1 + c_2 U_{11}^* + c_3 U_{11} \end{pmatrix} dh_{U(2)}(U) \tag{.6}$$

directly and, using the identities above, we obtain

$$\int_{U(2)} \det \mathfrak{D} \ dh_{U(2)} = c_1^2 - c_2 c_3. \tag{.7}$$

Similarly, we can expand the determinant in

$$\int_{U(3)} \det \begin{pmatrix} c_1 + c_2 U_{00}^* + c_3 U_{00} & c_2 U_{01}^* + c_3 U_{01} & c_2 U_{02}^* + c_3 U_{02} \\ c_2 U_{10}^* + c_3 U_{10} & c_1 + c_2 U_{11}^* + c_3 U_{11} & c_2 U_{12}^* + c_3 U_{12} \\ c_2 U_{20}^* + c_3 U_{20} & c_2 U_{21}^* + c_3 U_{21} & c_1 + c_2 U_{22}^* + c_3 U_{22} \end{pmatrix} dh_{U(3)}(U) \tag{.8}$$

using Sarrus' rule which yields (a few tedious pages later)

$$\int_{U(3)} \det \mathfrak{D} \ dh_{U(3)} = c_1^3 - 2 c_1 c_2 c_3 \tag{.9}$$

using the identities above.

For $SU(N)$, we have

- $p \neq q \;\Rightarrow\; \langle I, J | K, L\rangle = 0$
- $\langle | \rangle = 1$
- $\langle i, j | k, l\rangle = \frac{\delta_{il}\delta_{jk}}{N}$
- $\langle (i,j),(k,l)|\rangle = \langle |(i,j),(k,l)\rangle = -\frac{(-1)^{\delta_{ik}}}{2} = \frac{(-1)^{\varepsilon_{ik}}}{2}$ in $SU(2)$
- $\langle |(i,j,k),(l,m,n)\rangle = \langle (i,j,k),(l,m,n)|\rangle = \frac{\varepsilon_{ijk}\varepsilon_{lmn}}{6}$ in $SU(3)$

Hence, (analogous to the $U(N)$ computations)

$$\int_{SU(2)} \det \mathfrak{D}\; dh_{SU(2)} = c_1^2 + c_2^2 - c_2c_3 + c_3^2 \tag{.10}$$

and

$$\int_{SU(3)} \det \mathfrak{D}\; dh_{SU(3)} = c_1^3 - 2c_1c_2c_3 + c_2^3 + c_3^3. \tag{.11}$$

Appendix C: Proof of Corollary 2.3

By induction, we note for $2j < n$

$$\lim_{m\searrow 0} \frac{\tilde{m}_{2j-1}}{jm} = 1 \qquad \text{and} \qquad \lim_{m\searrow 0} \frac{\tilde{m}_{2j}}{\frac{1}{4jm}} = 1. \tag{.1}$$

This is trivially true for $\tilde{m}_1 = m$ and $\tilde{m}_2 = m + \frac{1}{4m}$. Then, we observe for $j > 1$

$$\lim_{m\searrow 0} \frac{\tilde{m}_{2j-1}}{jm} = \lim_{m\searrow 0} \frac{m + \frac{1}{4\tilde{m}_{2j-2}}}{jm} = \lim_{m\searrow 0} \frac{1}{j} + \frac{\frac{1}{4\tilde{m}_{2j-2}}}{jm} = \lim_{m\searrow 0} \frac{1}{j} + \frac{\frac{1}{4\frac{\tilde{m}_{2j-2}}{\frac{1}{4(j-1)m}}\frac{1}{4(j-1)m}}}{jm} \tag{.2}$$

$$= \frac{1}{j} + \frac{j-1}{j} = 1 \tag{.3}$$

and

$$\lim_{m\searrow 0} \frac{\tilde{m}_{2j}}{\frac{1}{4jm}} = \lim_{m\searrow 0} \frac{m + \frac{1}{4\tilde{m}_{2j-1}}}{\frac{1}{4jm}} = \lim_{m\searrow 0} 4jm^2 + \frac{jm}{\tilde{m}_{2j-1}} = 1. \tag{.4}$$

Thus, we obtain

$$\lim_{m\searrow 0} \tilde{m}_k\tilde{m}_{k+1} = \begin{cases} \lim_{m\searrow 0} \frac{\tilde{m}_k}{jm}\frac{\tilde{m}_{k+1}}{\frac{1}{4jm}}\frac{jm}{4jm} & ,\; k = 2j-1 \\ \lim_{m\searrow 0} \frac{\tilde{m}_k}{\frac{1}{4jm}}\frac{\tilde{m}_{k+1}}{(j+1)m}\frac{(j+1)m}{4jm} & ,\; k = 2j \end{cases} = \begin{cases} \frac{1}{4} & ,\; k = 2j-1 \\ \frac{j+1}{4j} & ,\; k = 2j \end{cases} \tag{.5}$$

and for $n \in 2\mathbb{N}$

$$\lim_{m\searrow 0} c_1 = \lim_{m\searrow 0} m\tilde{m}_n \prod_{j=1}^{\frac{n}{2}-1} \underbrace{\tilde{m}_{2j}\tilde{m}_{2j+1}}_{\to \frac{1}{4}\frac{j+1}{j}} \tag{.6}$$

$$= 2^{1-n} n \lim_{m\searrow 0} m\tilde{m}_n \tag{.7}$$

$$= 2^{1-n} n \lim_{m\searrow 0} m \left(m + \frac{1}{4\tilde{m}_{n-1}} + \sum_{j=1}^{n-1} \frac{(-1)^{j+1}4^{-j}}{m\prod_{k=1}^{j-1}\tilde{m}_k\tilde{m}_{k+1}} \right) \tag{.8}$$

$$= 2^{1-n} n \lim_{m\searrow 0} \left(\frac{\frac{n}{2}m}{4\tilde{m}_{n-1}}\frac{2}{n} + \sum_{j=1}^{n-1} \frac{(-1)^{j+1}4^{-j}}{\prod_{k=1}^{j-1}\tilde{m}_k\tilde{m}_{k+1}} \right) \tag{.9}$$

$$= 2^{1-n} n \left(\frac{1}{2n} + \lim_{m\searrow 0} \sum_{j=1}^{\frac{n}{2}} \frac{(-1)^{(2j-1)+1}4^{-(2j-1)}}{\prod_{k=1}^{(2j-1)-1}\tilde{m}_k\tilde{m}_{k+1}} + \sum_{j=1}^{\frac{n}{2}-1} \frac{(-1)^{2j+1}4^{-2j}}{\prod_{k=1}^{2j-1}\tilde{m}_k\tilde{m}_{k+1}} \right) \tag{.10}$$

$$=2^{1-n}n\left(\frac{1}{2n}+\sum_{j=1}^{\frac{n}{2}}\frac{4^{1-2j}}{\prod_{k=1}^{2(j-1)}\lim_{m\searrow 0}\tilde{m}_k\tilde{m}_{k+1}}-\sum_{j=1}^{\frac{n}{2}-1}\frac{4^{-2j}}{\prod_{k=1}^{2j-1}\lim_{m\searrow 0}\tilde{m}_k\tilde{m}_{k+1}}\right) \tag{.11}$$

$$=2^{1-n}n\left(\frac{1}{2n}+\sum_{j=1}^{\frac{n}{2}}\frac{4^{1-2j}}{4^{2-2j}\prod_{k=1}^{j-1}\frac{k+1}{k}}-\sum_{j=1}^{\frac{n}{2}-1}\frac{4^{-2j}}{4^{1-2j}\prod_{k=1}^{j-1}\frac{k+1}{k}}\right) \tag{.12}$$

$$=2^{1-n}n\left(\frac{1}{2n}+\sum_{j=1}^{\frac{n}{2}}\frac{1}{4j}-\sum_{j=1}^{\frac{n}{2}-1}\frac{1}{4j}\right) \tag{.13}$$

$$=2^{1-n}n\left(\frac{1}{2n}+\frac{1}{2n}\right) \tag{.14}$$

$$=2^{1-n}. \tag{.15}$$

Similarly, for $n\in 2\mathbb{N}-1$,

$$\lim_{m\searrow 0}c_1=\lim_{m\searrow 0}\tilde{m}_n\prod_{j=1}^{\frac{n-1}{2}}\underbrace{\tilde{m}_{2j-1}\tilde{m}_{2j}}_{\to\frac{1}{4}} \tag{.16}$$

$$=2^{1-n}\lim_{m\searrow 0}\left(m+\frac{4^{\frac{n-1}{2}}m}{4\frac{\tilde{m}_{n-1}}{\frac{1}{4^{\frac{n-1}{2}}m}}}+\sum_{j=1}^{\frac{n-1}{2}}\frac{4^{1-2j}}{m\prod_{k=1}^{2j-2}\tilde{m}_k\tilde{m}_{k+1}}-\sum_{j=1}^{\frac{n-1}{2}}\frac{4^{-2j}}{m\prod_{k=1}^{2j-1}\tilde{m}_k\tilde{m}_{k+1}}\right) \tag{.17}$$

$$=2^{1-n}\lim_{m\searrow 0}\left(\sum_{j=1}^{\frac{n-1}{2}}\frac{4^{1-2j}}{4^{2-2j}jm}-\sum_{j=1}^{\frac{n-1}{2}}\frac{4^{-2j}}{4^{1-2j}jm}\right) \tag{.18}$$

$$=0. \tag{.19}$$

Finally, the asserted identities for $Z(m,\mu,G,n)$ with $G\in\{U(1),SU(2),U(2),SU(3),U(3)\}$ are a trivial corollary substituting $\lim_{m\searrow 0}c_1$ into the formulae given in Theorem 2.2.